Near-infrared spectroscopy of nearby Seyfert galaxies. I. First results[⋆]

J. Reunanen[1], J.K. Kotilainen[1], M.A. Prieto[2]

[1] *Tuorla Observatory, University of Turku, Väisäläntie 20, FIN–21500 Piikkiö, Finland; reunanen@astro.utu.fi, jarkot@astro.utu.fi*
[2] *European Southern Observatory, Karl-Schwarzschild-Str. 2, D–85748 Garching bei München, Germany; aprieto@eso.org*

ABSTRACT

We present near-infrared $1.5 - 2.5$ μm moderate resolution long-slit spectra of two Seyfert 1 galaxies (NGC 1097 and NGC 1566), three Seyfert 2s (NGC 1386, NGC 4945 and NGC 5128) and one Seyfert 1.5 (NGC 3227), both parallel to ionization cone or jet and perpendicular to it. The spectra are used to study the spatial extent of the line emission, integrated masses of excited H_2 and the excitation mechanisms of interstellar gas. In all three Seyfert 2 galaxies, [Fe II] is found to be stronger than Brγ or H_2 1–0 S(1), while in the Seyfert 1 NGC 1566 and the Seyfert 1.5 NGC 3227 Brγ is the strongest line. Broad Brγ originating from the BLR is detected in three galaxies (NGC 1386, NGC 1566 and NGC 3227), of which NGC 1386 is optically classified as Seyfert 2. In these galaxies [Fe II] is narrow and may be X-ray excited. In all galaxies except in NGC 5128, the spatial FWHM size of H_2 1–0 S(1) nuclear core is larger perpendicular to the cone or jet than parallel to it, in agreement with AGN unified models. The values of nuclear N_{H_2} are higher in Seyfert 2s than in Seyfert 1s, with the Seyfert 1.5 NGC 3227 lying between them. The exception to this is the Seyfert 2 NGC 1386, where two extended regions are detected parallel to cone. Coronal lines are detected in two galaxies, NGC 1386 and NGC 3227.

Key words: galaxies:active – galaxies:nuclei – galaxies:Seyfert – infrared:galaxies

1 INTRODUCTION

Arguably the most important advance in recent research of active galaxies has been the development of unified models (e.g. Antonucci 1993), where a thick molecular torus surrounds the nucleus. In Seyfert 1 (Sy1) galaxies the nucleus and the Broad Line Region (BLR) are directly visible, while in Seyfert 2 (Sy2) galaxies the torus obscures the nucleus and the BLR and only the Narrow Line Region (NLR) is visible. These models are supported by the detection in many Sy2s of broad lines in polarized emission (e.g. Moran et al. 2000), believed to be light from the BLR reflected into our line-of-sight, and cone-like structures in narrow-band [O III] images (e.g. Mulchaey, Wilson & Tsvetanov 1996) almost invariably aligned with the radio jets.

Searches for the obscuring molecular material associated with the torus have mostly been carried out at millimeter wavelengths (e.g. Maiolino et al. 1997), and consequently they generally give only the total molecular content in the nucleus. Better spatial resolution, and therefore smaller contamination from any circumnuclear star formation, can be achieved by observing in the near-infrared (NIR; e.g. Veilleux, Goodrich & Hill 1997), where in addition to the molecular H_2 lines a wealth of other emission and absorption lines are available. However, the NIR spectroscopic studies have mostly been made at moderate spatial resolution ($>1''.5$). Only recently have better resolution NIR studies been carried out (e.g. Storchi-Bergmann et al. 1999, Winge et al. 2000), but even these studies have only one slit position angle (PA) along either the radio axis or the major axis of inner isophotes in [O III] images, and thus can not derive the geometry of the molecular emission.

In this paper we present the results of long-slit 1.5–2.5 μm moderate resolution spectroscopy of the first six galaxies in our sample of nearby ($500 < v < 1500$ km s^{-1}) Seyfert galaxies of both types with an ionization cone and/or jets. The slit was positioned both perpendicular and parallel to the ionization cone or to the jet in order to probe the distribution of the molecular material and thus the geometry of the torus. Additionally, broad-band JHK'-images are available for all the galaxies. These data are used to trace the spatial distribution, dynamics and excitation of molecular

---

and nebular gas, and to determine the mass of hot ($T > 1000$ K) molecular gas in the central regions.

In forthcoming publications, we shall discuss the implications from the emission line study of all the 14 Seyferts in our sample, and study the stellar populations and star forming histories of the sample, based on the absorption lines, and comparison with non-Seyfert spirals.

This paper is organized as follows: In Section 2 the observations, data reduction and methods used in the analysis are outlined. In Section 3 the galaxies are discussed individually, and in Section 4 we present our preliminary conclusions. Throughout this paper, $H_0 = 75$ km s^{-1} Mpc^{-1} and $q_0 = 0.5$ are assumed.

2   OBSERVATIONS, DATA REDUCTION AND METHODS OF ANALYSIS

Six nearby active galaxies were observed in January 1999 with the 3.6 m ESO New Technology Telescope (NTT) using the 1024×1024 px SOFI camera (Lidman, Cuby & Vanzi 2000)and a pixel scale $0\rlap{.}''29$ px^{-1}. The best, average and worst seeing during the observations were $0\rlap{.}''65$, $\sim1\rlap{.}''0$ and $1\rlap{.}''35$, respectively. In the spectroscopic observations the red grism with resolution $R = 980$ and slit width $1\rlap{.}''0$ ($0\rlap{.}''6$ for NGC 1386) were used. The wavelength range covered is 1.5–2.5 μm and the useful slit length $\sim2'$. Broad-band $JHKs$ images were also obtained, except for NGC 1097, for which we used the image presented in Kotilainen et al. (2000). The properties of the galaxies, redshift, scale, inclination, PA of the major axis, morphology, AGN type, the PAs used, total integration times, slit width and FWHM seeing, are given in Table 1.

The long-slit spectra were taken parallel and perpendicular to the PA of the cone or jet. The integrations were taken in two positions along the slit separated by $\sim2'$ and the pairs were subtracted from each other. The images were then flat-fielded using dome flats. Bad pixels were masked out and any remaining cosmic rays were removed manually. The images were wavelength calibrated using either OH night sky lines or Xe arc lamp calibration frames. The nucleus was traced by fitting a low order polynomial, a strip was extracted, and the strips were averaged to erase the residual continuum and OH lines from the sky. Finally, the images were divided by an atmospheric standard star, flux calibrated and averaged. IRAF† was used for all stages of the data reduction.

The accurate determination of fluxes and line widths requires a good S/N ratio, and therefore two or more pixels were binned together. However, the sizes given later for the nuclear sources are based on unbinned data. In order to probe the nuclear region as deeply as possible, all the spectra of a given galaxy were combined and the central $1\rlap{.}''5$ (5 px) spectrum was extracted. As a result of this and the slit width ($1\rlap{.}''0$ or $0\rlap{.}''6$), the effective aperture has a diameter of $1\rlap{.}''4$ or $1\rlap{.}''1$. The fluxes and widths of the lines detected in this aperture are given in Table 2. For few lines, especially

---

† IRAF is distributed by the National Optical Astronomy Observatories, which are operated by the Association of Universities for Research in Astronomy, Inc., under cooperative agreement with the National Science Foundation

for [Ca VIII] in NGC 1386, an outlaying region with no line emission was subtracted to remove the underlaying absorption lines. The quoted errors in the following sections are generally dominated by the continuum fitting, and are 1σ except 3σ for upper limits.

2.1   Extinction

We have estimated the extinction by comparing the observed integrated colours from the spectra with the colours of normal, unobscured spiral galaxies (H-$K = 0.22$, Hunt et al. 1997), as the H-K color of S0 or E galaxies resemble the color of spiral galaxies (Fioc & Rocca-Volmerange 1999). We note that the extinction based on continuum colours or the slope of the spectra may not be correct for the line emission. However, no useful line pairs were generally detected. Only in NGC 4945 the Brζ and Brη lines are visible in a few regions and the extinction based on them is similar to that derived from the continuum colours of the spectra. The difficulty of detecting other H II lines arises from the high extinction these galaxies suffer, the intrinsic weakness of the H II lines and/or the contamination from nearby absorption lines. We have assumed the extinction law $A_\lambda \propto \lambda^{-1.85}$ (Landini et al. 1984) and a foreground dust screen. The extinction is given in Table 2 for the central region and in the lowest panel of the spatial profile figures. Our extinction measurements are in fairly good agreement with the previous derivations: e.g. in NGC 4945 Marconi et al. (1996) derived $A_V \sim 1.1$ from the continuum colors and $A_V > 1.3$ in the Paα ring. The observed colors are also in agreement with previous measurements (e.g. H-$K = 0.34$ Kotilainen et al. 2000; here 0.37).

In addition to the hydrogen recombination lines, [Fe II] lines can be used to estimate the extinction. A useful line pair in the 1.5-2.5 μm range is 1.5339 and 1.6773 μm, which originate from the same ^{4}D$_{5/2}$ level. These faint emission lines are detected in NGC 1386, NGC 1566, NGC 3227 and NGC 5128, as marked in the respective figures. However, the lines are generally much broader and more extended than the main 1.64 μm line. For this reason, they have not been used in the analysis. These features are not artificial or telluric as the velocity field derived from them agrees with the general rotation of the galaxies.

2.2   H$_2$ molecular gas: excitation and mass estimate

The emission line ratios can be used to probe the excitation mechanisms of the interstellar matter. Sources of line emission can roughly be divided into three classes: cool or warm molecular clouds (H$_2$ lines), warm ionized interstellar gas (H II lines, [Fe II], He I) and very hot, highly ionized matter near the centre of the galaxies (coronal lines). The main mechanisms for the H$_2$ emission are thermal (collisional) heating and UV pumping (fluorescence). Thermal excitation, either by shocks (e.g. Hollenbach & McKee 1989), by UV radiation in dense ($n \geqslant 10^4$ cm^{-3}) clouds (Sternberg & Dalgarno 1989) or by X-rays (e.g. Gredel & Dalgarno 1995), is preferred as the dominant mechanism in most extragalactic sources.

The H$_2$ line ratio 2–1 S(1)/1–0 S(1) is commonly used
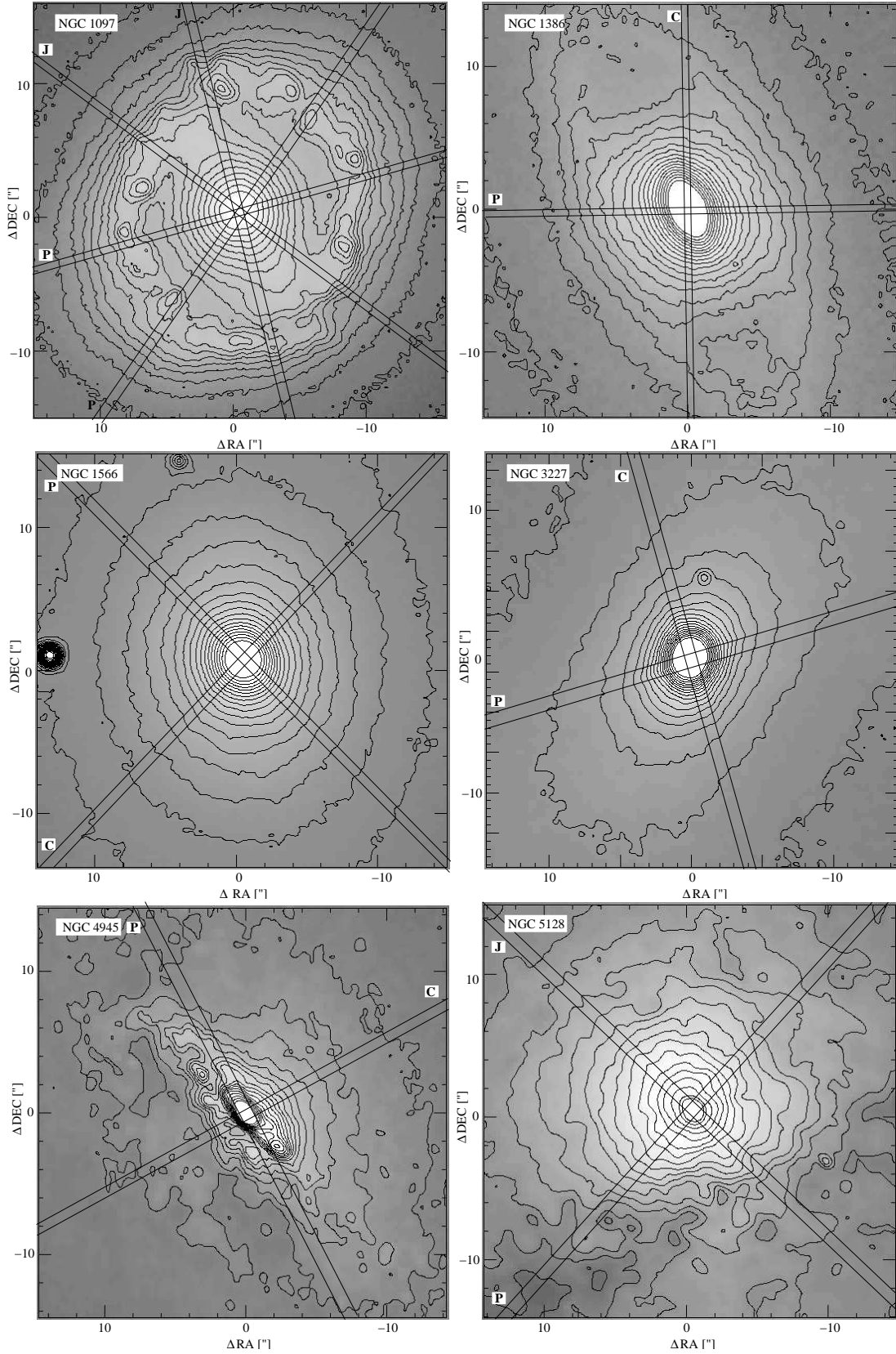
Figure 1. The *K*-band image of NGC 1097 (*upper left*) from Kotilainen et al. (2000), and the *Ks*-band images of NGC 1386 (*upper right*), NGC 1566 (*middle left*), NGC 3227 (*middle right*), NGC 4945 (*lower left*) and NGC 5128 (*lower right*). North is up and East to the left. Slit positions are indicated in the images, marked with C for parallel to the cone on the side where the cone is stronger, J parallel to the jet and P perpendicular to them.

Table 1. Observational properties of the galaxies.

Galaxy	z	Scale pc/''	i °	PA °	Morphology	Nucleus	PA$_{\parallel}$ °	PA$_{\perp}$ °	t_{int} min	Slit width ''	Seeing ''
NGC 1097	0.00425	82	46	141	SB(s)b	Sy1	15,54	-36,-75	2×32,2×48	1''0	1''0
NGC 1386	0.00289	56	74	25	SB0^{+}	Sy2	1	-89	48,64	0''6	1''1
NGC 1566	0.00483	94	28	30	SAB(s)bc	Sy1	-42	48	48,64	1''0	1''0
NGC 3227	0.00382	74	56	158	SAB(s)a pec	Sy1.5	15	-75	48,80	1''0	1''0
NGC 4945	0.00194	19	78	43	SBcdsp	Sy2	-64	26	32,64	1''0	0''9
NGC 5128	0.00179	19	65	30	E2	Sy2	50	-40	16,48	1''0	0''9
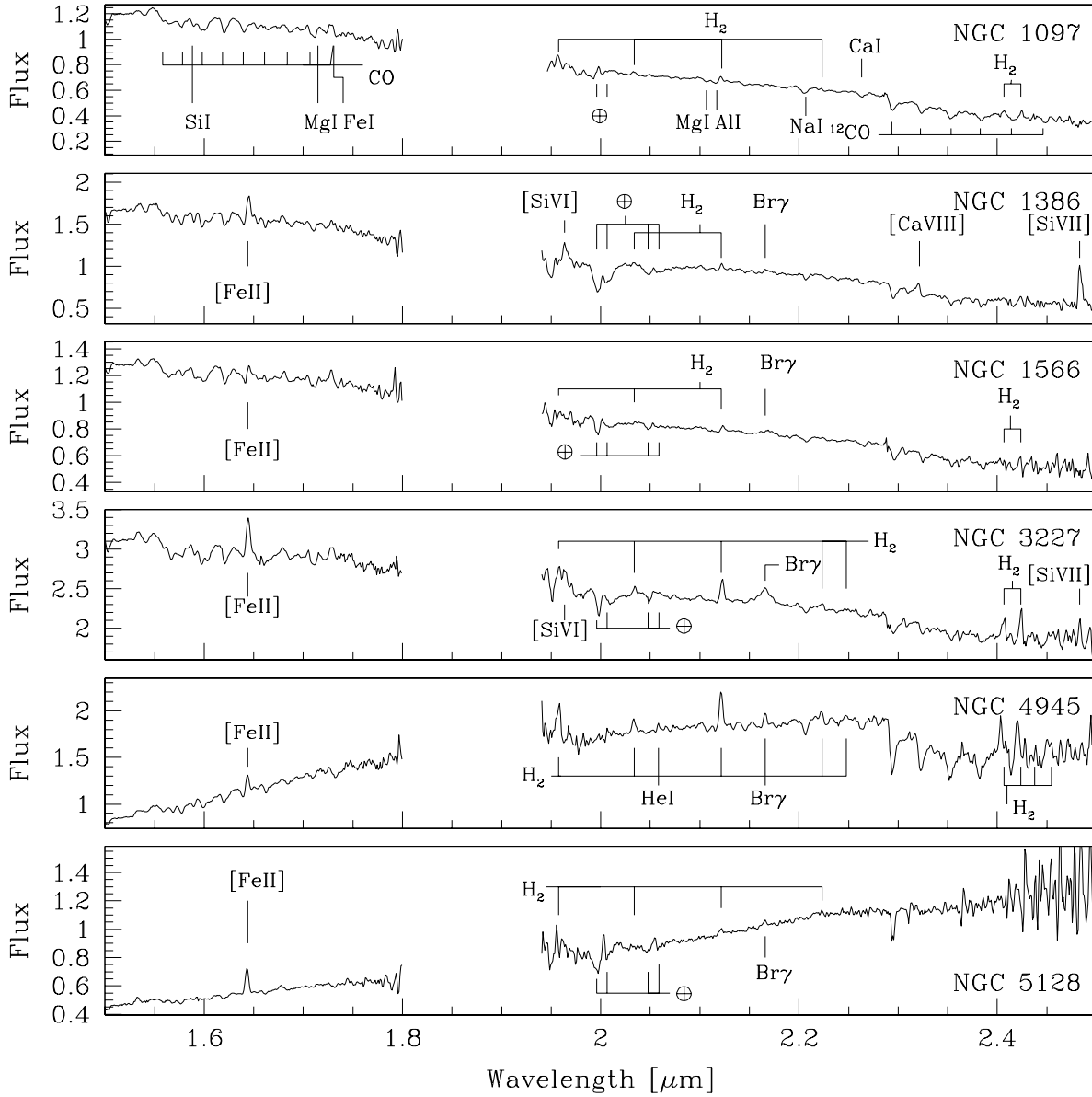
Figure 2. The nuclear H- and K-band spectra in a 1''4 (1''1 for NGC 1386) aperture for, from top to bottom, NGC 1097, NGC 1386, NGC 1566, NGC 3227, NGC 4945 and NGC 5128. The flux units are 10^{-15} ergs s^{-1} cm^{-2} Å^{-1}. The main emission lines are marked in each panel, and absorption lines in the first panel. Atmospheric features are marked with $\oplus$.
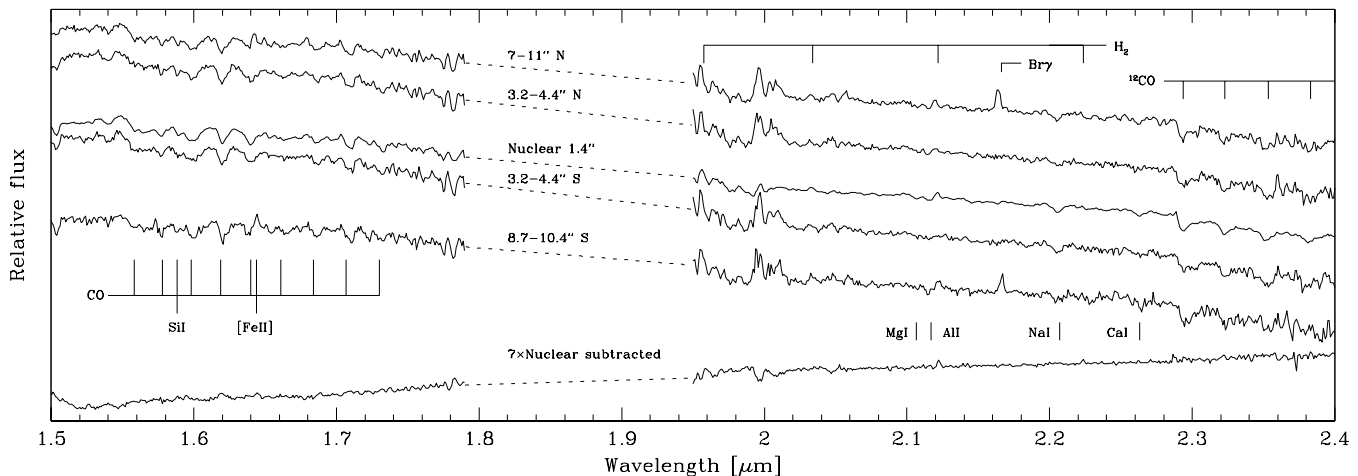
Figure 3. The 1.5–2.5 μm spectrum of NGC 1097 at PA=15°(parallel to the jet) at different positions along the slit. The K-band flux was scaled to match the flux in nuclear 1$''$4 aperture, and the spectra were placed at uniform intervals to facilitate comparison between different regions. The absorption features at 2.0 μm and 2.05 μm are due to poor atmospheric cancellation. The nuclear subtracted spectrum was obtained as discussed in the text.

to distinguish between thermal ($\sim$0.1–0.2) and UV ($\sim$0.55) excitation in low density regions. Interpretation of the H_2 2–1 S(1)/1–0 S(1) ratio is somewhat hampered, if X-rays play a significant role in the excitation of the molecular gas (Maloney, Hollenbach & Tielens 1996). Qualitative estimation for the importance of X-ray excitation can be derived from the strength of [Fe II]; X-ray excitation predicts [Fe II]/Brγ up to $\sim$20, while H II regions have [Fe II]/Br$\gamma < 2.5$ (Alonso-Herrero et al. 1997). The ratio 2–1 S(1)/1–0 S(1) is later used to derive the vibrational excitation temperature T_{vib} ($T_{vib} \simeq 5600/\ln(1.355 \times I_{1-0S(1)}/I_{2-1S(1)})$) assuming Einstein A-terms by Turner, Kirby-Docken & Dalgarno 1977), while the rotational temperature is generally derived from the line ratio 1–0 S(0)/1–0 S(2) ($T_{rot} \simeq -1113/\ln(0.323 \times I_{1-0S(2)}/I_{1-0S(0)})$).

The equation for the mass of the excited molecular hydrogen can be derived assuming $T = 2000$ K, the 1–0 S(1) transition probability $A_{S(1)} = 3.47 \times 10^{-7}$ s^{-1} (Turner et al. 1977) and the population fraction in the $\nu = 1$, $J = 3$ level $f_{\nu=1,J=3} = 0.0122$ (Scoville et al. 1982)

$$m_{H_2} \simeq 5.0875 \times 10^{13}\, D^2\, I_{1-0S(1)}\, 10^{0.4277 A_{2.2}}$$

where m_{H_2} is the mass of the excited H_2 in $M_\odot$, D is distance in Mpc, $I_{1-0S(1)}$ is the observed flux in ergs cm^{-2} s^{-1} and $A_{2.2}$ is the 2.2 μm extinction. Integrated masses were derived for all PAs (Table 3). Since the effective length of the slit is $\sim$2$'$, the slit covers most of the galaxy and the inclination effect is negligible. We have also determined the average surface density and the mass of the excited H_2 in the nucleus. As our nuclear aperture is not significantly larger than the seeing, the average surface density can then be used to compare the amount of molecular material between Sy1s and Sy2s.

3 RESULTS AND DISCUSSION

The nuclear $30\times30''$ images of the galaxies are displayed in Fig. 1 and the H- and K-band nuclear spectra in Fig. 2. We were unable to completely remove the telluric features at ~ 2.0 μm and ~ 2.05 μm. These signatures are due to H_2O and are not only temporally but also spatially variable so they can not be removed by self-calibration with a distant region in the galaxy.

3.1 NGC 1097

NGC 1097 is a nearby (distance = 17 Mpc) SB(s)b galaxy with a strong bar at PA $\sim$137°. It interacts with a small elliptical companion toward NW. NGC 1097 has an almost circular starburst ring (diameter 1.5-kpc) and a nuclear bar, visible both in the NIR continuum (Fig. 1) and in the 1–0 S(1) line emission (Kotilainen et al. 2000). In the optical, NGC 1097 has four faint straight jets (e.g. Wehrle, Keel & Jones 1997). Originally thought to be a LINER (Phillips et al. 1984), currently NGC 1097 is classified as a Sy1, based on the detection of broad, variable double-peaked Hα emission (Storchi-Bergmann, Baldwin & Wilson 1993). The radio nucleus of NGC 1097 is compact and weak (Wolstencroft, Tully & Perley 1984). To our knowledge, this is the first HK-band spectroscopic study of NGC 1097.

The H- and K-band spectra of NGC 1097 at PA 15° are shown in Fig. 3. The nuclear subtracted spectrum shown has been obtained by matching the flux of the K-band CO lines in the off-nuclear (0$''$7-1$''$6 from the nucleus) spectra to 1$''$4 nuclear aperture and subtracting the result from the nuclear spectra. The subtracted spectrum is included here to better show the weak nuclear emission lines, especially in the case of NGC 1386 discussed later. The full discussion and analysis of the subtracted spectra are postponed to forthcoming papers. The only emission lines directly detected in the nucleus are the various H_2 lines (Table 2). This agrees with the results of Kotilainen et al. (2000), who detected nuclear

Table 2. Observed fluxes within the nuclear $1''\!\!.4$ ($1''\!\!.1$ for NGC 1386) aperture, after adding all the data from different slit PAs. The fluxes (first row) are in units of 10^{-15} ergs cm^{-2} s^{-1} and the FWHMs (second row) in Å. A reliable estimate for the 1–0 S(3) emission in NGC 3227 is impossible due to telluric residuals.

Line	λ	NGC 1097 Sy1	NGC 1386 Sy2	NGC 1566 Sy1	NGC 3227 Sy1.5	NGC 4945 Sy2	NGC 5128 Sy2
A$_{2.2}$		0.23	0.26	0.37	0.71	1.82	1.62
[Fe II]	1.644	0.57±0.14	10.2±0.32	2.13±0.13	20.8±0.28	6.26±0.20	23.1±0.35
		32±8	38±1	33±2	41±1	32±1	40±1
1–0 S(3)	1.9576	2.92±0.07	<0.4	0.7±0.2		17.0±0.26	7.30±0.20
		33±1		22±3		45±1	22±1
[Si VI]	1.9635	<0.3	10.1±0.18	<0.3	6.9±0.2	<0.5	<0.7
			44±1		31±1		
1–0 S(2)	2.0338	1.27±0.05	1.38±0.11	0.29±0.03	4.78±0.12	6.30±0.10	<0.6
		43±2	30±2	11±2	37±1	40±1	
He I	2.0581	<0.2	<0.3	<0.2	<0.3	1.54±0.09	<0.6
						21±1	
1–0 S(1)	2.1218	1.32±0.04	1.98±0.09	1.53±0.03	11.6±0.08	15.2±0.10	8..41±0.19
		30±1	26±1	35±1	36±1	36±1	37±1
Brγ	2.1661	<0.30	1.76±0.14	5.60±0.10	22.1±0.18	5.23±0.10	4.40±0.20
			64±3	137±5	125±1	34±1	36±2
1–0 S(0)	2.2235	0.45±0.05	<0.3	<0.2	3.34±0.11	3.00±0.09	1.62±0.08
		22±2			31±1	30±1	17±1
2–1 S(1)	2.2477	<0.2	<0.3	<0.2	0.93±0.08	2.08±0.10	<0.52
					29±2	34±1	
[Ca VIII]	2.3213	<0.2	3.78±0.14	<0.3	<0.3	<0.40	<0.6
			43±2				
1–0 Q(1)	2.4066	1.67±0.15	<0.5	0.92±0.22	10.5±0.15	12.4±0.11	<0.9
		34±3		11±4	39±1	30±1	
1–0 Q(3)	2.4237	2.40±0.13	<0.5	2.35±0.14	14.3±0.14	13.5±0.11	<0.9
		30±2		27±2	30±1	32±1	
[Si VII]	2.4833	<1.1	17.8±0.40	<1.70	6.1±0.3	<0.90	<1.5
			38±1		20±1		

Table 3. The column density of the excited H$_2$, line ratios, the integrated H$_2$ mass, the nuclear spatial extent and the total extent of the lines for the sample galaxies, both parallel to the cone/jet ($\parallel$) and perpendicular to it ($\perp$). The spatial extent (FWHM) is measured from unbinned data in the plane of the sky and is corrected for instrumental resolution. The total extent is given in the plane of the galaxy. M$_{H_2}$ and extent in NGC 1097 are given within the ring.

| Galaxy	NGC 1097	NGC 1386	NGC 1566	NGC 3227	NGC 4945	NGC 5128
Nucleus	Sy1	Sy2	Sy1	Sy1.5	Sy2	Sy2
Aperture	$1''\!\!.4$	$1''\!\!.1$	$1''\!\!.4$	$1''\!\!.4$	$1''\!\!.4$	$1''\!\!.4$
N$_{H_2}$ [10^{17} cm^{-2}]	1.5	3.7	1.9	22.3	100	44
M$_{H_2}$ [M$_\odot$]	25	17	42	280	70	32
[Fe II]/1–0 S(1)	0.50	6.1	1.5	2.8	1.20	7.3
Brγ/1–0 S(1)	...	0.88	2.7	1.9	0.32	0.49
1–0 S(0)/1–0 S(1)	0.33	<0.15	<0.15	0.27	0.17	0.17
1–0 S(2)/1–0 S(1)	0.98	0.72	0.20	0.44	0.49	<0.09
2–1 S(1)/1–0 S(1)	<0.15	<0.15	<0.15	0.08	0.12	<0.06
M$_{H_2}$ $\perp$ [M$_\odot$]	60	30	110	340	190	30
M$_{H_2}$ $\parallel$[M$_\odot$]	90	50	90	300	90	30
T$_{vib}$ [K]	<2550	<2500	<2700	1950	2200	<1800
FWHM 1–0 S(1) $\perp$ [pc]	108	39	82	84	57	35
FWHM 1–0 S(1) $\parallel$ [pc]	99	...	65	58	28	42
FWHM [Fe II] $\perp$ [pc]	...	...	...	43	50	...
FWHM [Fe II] $\parallel$ [pc]	...	...	...	51	50	...
Extent 1–0 S(1) $\perp$ [pc]	80	190	280	860	1160	720
Extent 1–0 S(1) $\parallel$ [pc]	340	410	210	600	1560	240
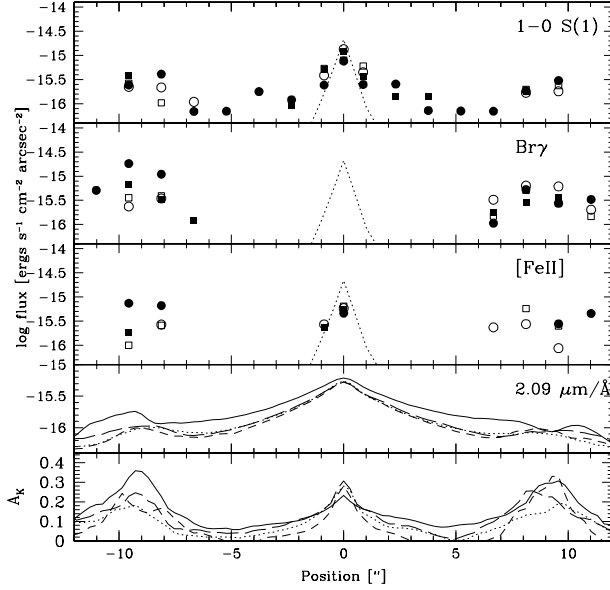
Figure 4. The observed line emission in NGC 1097. Open symbols indicate perpendicular to the jets (PA of squares = -36°, PA of circles = -75°) and filled symbols parallel to the jets. The PSF is indicated by dotted lines. The 2.09 μm continuum emission (fourth panel) and extinction (fifth panel) are shown for the PAs of 15°(solid line), 54°(dotted line), -75°(short-dashed line) and -36°(long-dashed line). The positive locations along the slit are in S (PA=15°), SW (54°), SE (-36°) and E (-75°).
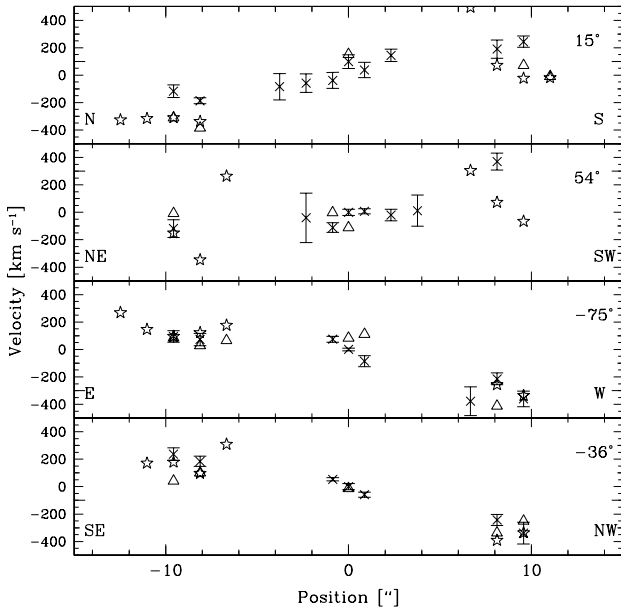

Figure 5. The velocity field of NGC 1097 in the most important emission lines in the units of km s^{-1}, 1–0 S(1) (crosses), Brγ (stars) and [Fe II] (triangles).

1–0 S(1) but no Brγ emission in their narrow-band images, suggesting that thermal UV heating is not important. The 1–0 S(1) emission is detected further away from the nucleus parallel to jets than perpendicular to them (see Fig. 4). Parallel to jets it can be followed up to 2–3″ ($\sim$280 pc in the plane of the galaxy) from the nucleus while perpendicular to them only up to $\sim$1″ ($\sim$90 pc) (Table 3), in agreement with the 1–0 S(1) image of Kotilainen et al. (2000). The distances quoted are corrected for inclination taking into account the position angle of the slit unless otherwise stated.

In the *H*-band (Fig. 3), [Fe II] can only be detected after subtracting the underlying CO features. The [Fe II] line is narrow (intrinsic FWHM 400 km s^{-1}), although wider than in typical starbursts ($\lesssim$ 300 km s^{-1}; e.g. Moorwood & Oliva 1988). The 1–0 S(1) line is narrower than [Fe II], with intrinsic FWHM 270 km s^{-1}. No 2–1 S(1) emission is detected, with 2–1 S(1)/1–0 S(1) < 0.13 (assuming $T_{\rm vib}$ < 2400 K) in the central 1″4 aperture, indicating that fluorescent excitation cannot be significant. We conclude that in the nucleus there is no current star formation and the H$_2$ gas is collisionally excited.

The derived parameters, including the density and mass of molecular hydrogen and the spatial extent of different lines in NGC 1097 are given in Table 3. In the nuclear 1″4 aperture, the column density of excited molecular hydrogen is 1.5×10^{17} cm^{-2} (corresponding to $M_{\rm H_2} = 25$ M$_\odot$), assuming $T = 2000$ K. The integrated mass of excited H$_2$ inside the starburst ring is larger parallel to the jets (40 and 50 M$_\odot$) than perpendicular to them ($\sim$30 M$_\odot$). This suggests that H$_2$ emission is produced by shocks in the jets. However, further away in the galaxy H$_2$ emission was not detected, while the optical jets continue much further. This discrepancy is in agreement with the non-detection of optical emission lines in the jets (Wehrle et al. 1997).

The kinematics of NGC 1097 has been discussed in detail by Storchi-Bergmann, Wilson & Baldwin (1996a), who found the starburst ring to be located between the inner Lindblad resonances. Our NIR velocity fields (Fig. 5) are in good agreement with their Hα velocity field. There are no significant differences between the kinematics of H$_2$, Brγ or [Fe II].

3.2 NGC 1386

NGC 1386 is a nearby (distance = 11.5 Mpc) SB0$^+$ galaxy in the Fornax cluster with a Sy2 nucleus and dust lanes across the nuclear region (e.g. Malkan, Gorjian & Tam 1998). NGC 1386 has a star forming ring with major axis diameter $\sim$1.3-kpc (Weaver, Wilson & Baldwin 1991). The nuclear radio core (Nagar et al. 1999) is extended in PA$\sim$ 170°, which is different from the optical major axis PA ($\sim$ 25°). Weaver et al. (1991) detected an outflow directed along the major axis. Low-resolution ($R = 250$) *JHK*-spectra were taken by Winge et al. (2000). The [O III] image of Storchi-Bergmann et al. (1996b) has a separate emission region to N. The slit was aligned to include this region.

The *H*- and *K*-band spectra of NGC 1386 along the cone are shown in Fig. 6, while the extent of the lines is displayed in Fig. 7. While Brγ and [Fe II] are only marginally resolved, the 1–0 S(1) emission is extended parallel to the cone, where the two clearly detected separate regions are discussed in detail below. The H$_2$ emission can be traced $\sim$4″5
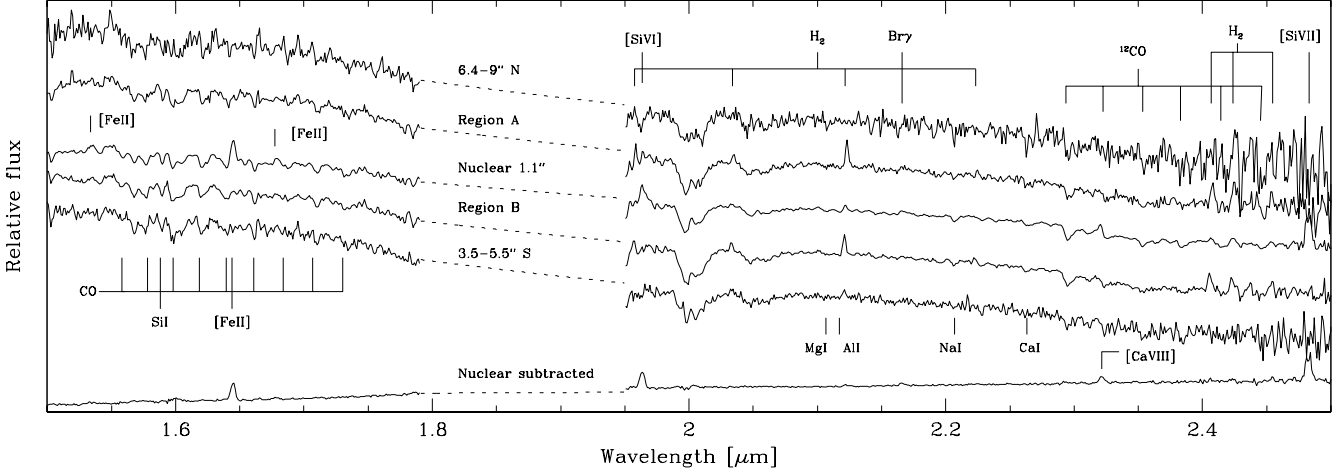
Figure 6. The $1.5 - 2.5$ μm spectra of NGC 1386 parallel to the cone.

(440 pc in the plane of the galaxy) towards N and $\sim 3''.5$ (340 pc) towards S. The nuclear 1–0 S(1) core is not resolved parallel to the cone, while in the perpendicular direction it is marginally resolved. There is no extended emission perpendicular to the cone.

Three spatially unresolved coronal lines ([Si VI] 1.9635 μm, [Ca VIII] 2.3213 μm and [Si VII] 2.4833 μm) are detected in the nucleus of NGC 1386 (Fig. 6). Strongest of these coronal lines is [Si VII] and it is also overall the strongest observed line in the nuclear spectrum. Previously, the [Ca VIII] coronal line has only been detected in the Sy2s Circinus (Oliva et al. 1994) and NGC 1068 (Marconi et al. 1996), and unlike in them, [Ca VIII] in NGC 1386 is already clearly visible before the underlying CO features have been subtracted (Fig. 6). There is a red wing in both [Si VII] and [Si VI], and possibly in [Ca VIII], after the CO absorption features have been subtracted. The [Si VI]/[Si VII] ratio in the nucleus is 0.48, compatible either with shocks with relatively little contribution from UV excitation, or with strong UV continuum excitation (Contini & Viegas 2001).

We did not detect 2–1 S(1) nor 1–0 S(0) emission in the nucleus. The upper limit to 2–1 S(1)/1–0 S(1) ratio, $\leqslant 0.12$, is compatible with thermal excitation with $T_{\mathrm{vib}} \leqslant 2310$ K. Assuming $T_{\mathrm{vib}} = 2000$ K, we derive $N_{\mathrm{H_2}} = 3.9 \times 10^{17}$ cm^{-2} (corresponding to $M_{\mathrm{H_2}} \simeq 20$ M$_\odot$) within the nuclear $1''.1$ aperture. The 1–0 S(1)/Brγ ratio is 1.14, strongly suggesting that thermal UV heating is insignificant, as then Brγ should be much stronger. On the other hand, the [Fe II]/Brγ ratio is 7.1, suggesting a significant contribution from X-rays to the ionization. Since the Brγ is broad, the ratios derived above are in fact lower limits. The likely excitation mechanism for nebular gas is therefore X-rays, further supported by the much larger width of [Fe II] (560 km s^{-1}) and Brγ ($\sim$800 km s^{-1}) compared to 1–0 S(1) (190 km s^{-1}).

The Brγ line is broad and asymmetric (Fig. 8), while both 1–0 S(1) and [Fe II] emission are symmetric. Brγ is broader than the optical lines (e.g. Rossa, Dietrich & Wagner 2000), and is likely to originate from the BLR. There is no corresponding broad component to the [Fe II] line, so the observed [Fe II] emission arises outside the BLR. Brγ is concentrated in the nucleus, and the strong Hα peak (Rossa et
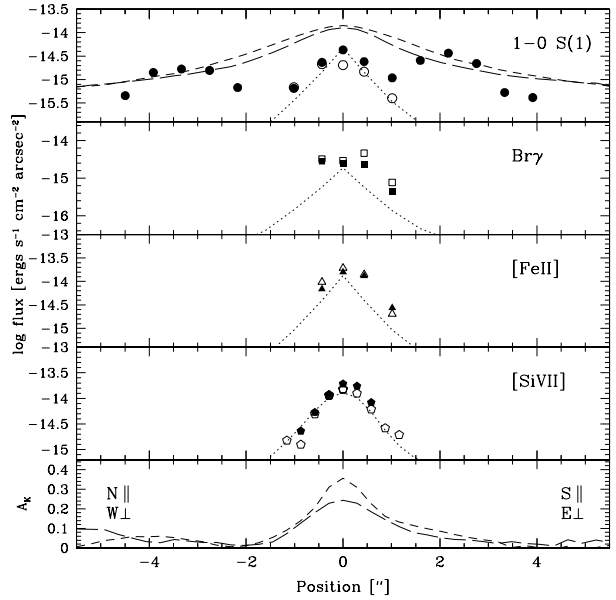

Figure 7. The observed line emission in NGC 1386 perpendicular to the ionization cone (open symbols) and parallel to it (filled symbols). The PSF (dotted line) and the 2.09 μm continuum emission multiplied by 10 are also shown. In the lowest panel the extinction is shown parallel to the cone (short-dashed line) and perpendicular to it (long-dashed line).

al.) is not detected in Brγ, demonstrating the reduced effect of extinction in the NIR. There is no detectable emission from the starburst ring, which is not surprising considering its faintness (only a few % of the brightness of the nucleus in Hα; Storchi-Bergmann et al. 1996b). However, the ring is visible in the K'-band (Fig. 1).

The velocity field of NGC 1386 is displayed in Fig. 9. The H$_2$ rotation curve is relatively ordered parallel to the cone, suggesting that circular motions dominate the kinematics.
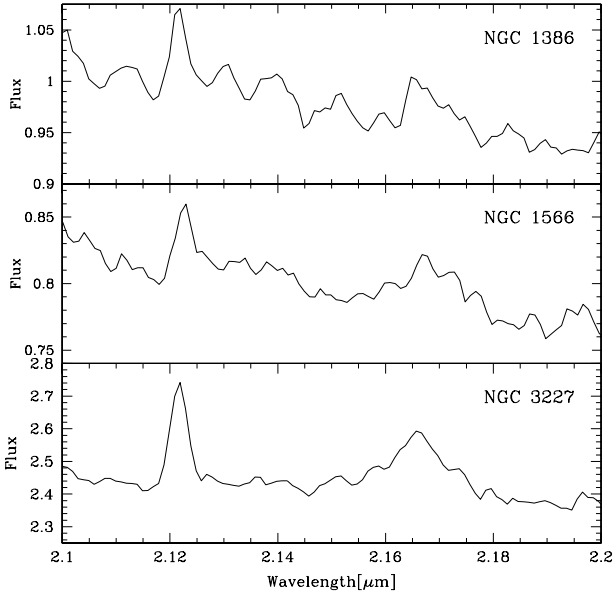
Figure 8. Enlarged spectral area around 2.15 μm showing broad Brγ and narrow 1–0 S(1) for NGC 1386, NGC 1566 and NGC 3227 from top to bottom, respectively, in $1''\!.4$ ($1''\!.1$ for NGC 1386) aperture in units of 10^{-15} ergs s^{-1} cm^{-2} Å^{-1}

3.2.1 Two extended regions parallel to the cone

The most interesting features in Fig. 7 are the two extended H$_2$ emission regions parallel to the cone. Region A covers the area $4''\!.4 - 2''\!.3$ to the north and region B $1''\!.1 - 3''\!.2$ to the south of the nucleus. Neither of the regions is visible in the broad–band images. Extinction derived from continuum colours is $A_{2.2} = 0.03$ and $A_{2.2} = 0.09$ mag, while that derived from the 1–0 Q(3)/1–0 S(1) ratio is $A_{2.2} = 0.04$ and $A_{2.2} = 0.20$. for regions A and B, respectively. The H$_2$ lines in these two regions are narrower than in the nucleus (Table 4), in contrast to the situation in NGC 4945 (Section 3.5).

Many of the weaker H$_2$ lines not detected in the nucleus are visible in the two regions due to much fainter continuum in these regions than in the nucleus, while the line fluxes are comparable to those in the nucleus. The line widths are only slightly larger than the instrumental resolution (~ 22 Å). The 2–1 S(1) line was not detected in either region, setting upper limits of $T_{\rm vib}$ as 2600 K and 2100 K for regions A and B, respectively. Furthermore, the non-detection of Brγ suggests thermal excitation in shock-heated clouds. The 1–0 S(0)/1–0 S(2) ratio is 0.60 and 0.46 for regions A and B, respectively, and is compatible with $T_{\rm rot} \simeq 1800$ K or 3200 K. For region A, this temperature is in good agreement with the 2–1 S(1)/1–0 S(1) upper limit ($T_{\rm vib} < 2100$ K) assuming thermal excitation. For region B, the two derived temperatures agree within errors.

The mass of the excited molecular hydrogen associated with the two regions of $2''\!.3\times0''\!.6$ ($\sim$4350 pc^2) area is $\sim$10 M$_\odot$ ($N_{\rm H_2} = 1.9\,10^{17}$ cm^{-2}) and $\sim$30 M$_\odot$ ($3.8\,10^{17}$ cm^{-2}), for regions A and B, respectively. These masses are comparable to the mass within the $1''\!.1$ nuclear aperture, $\sim$20 M$_\odot$.
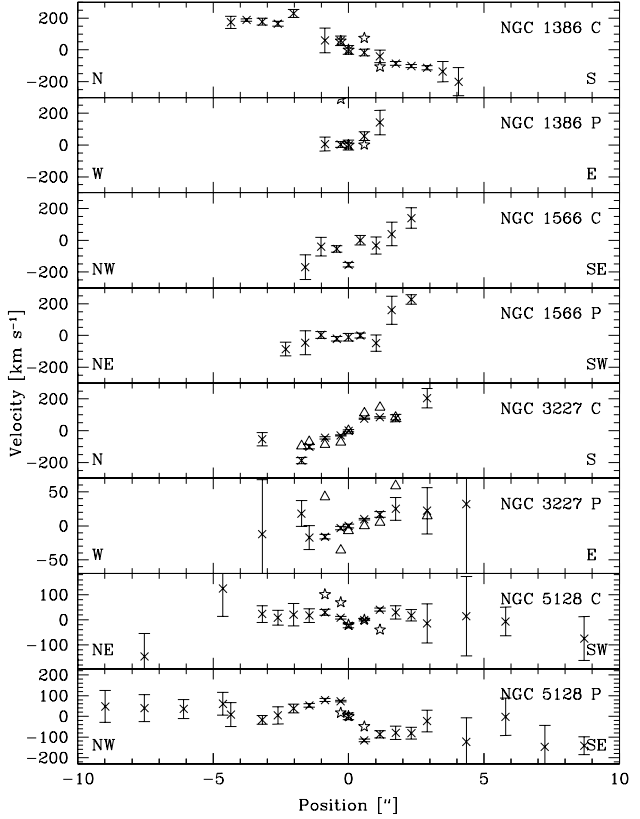

Figure 9. The 1–0 S(1) (crosses with errorbars), [Fe II] (triangles) and Brγ (stars) velocity curves for NGC 1386, NGC 1566, NGC 3227 and NGC 5128 parallel to the cone (C) and perpendicular to it (P)
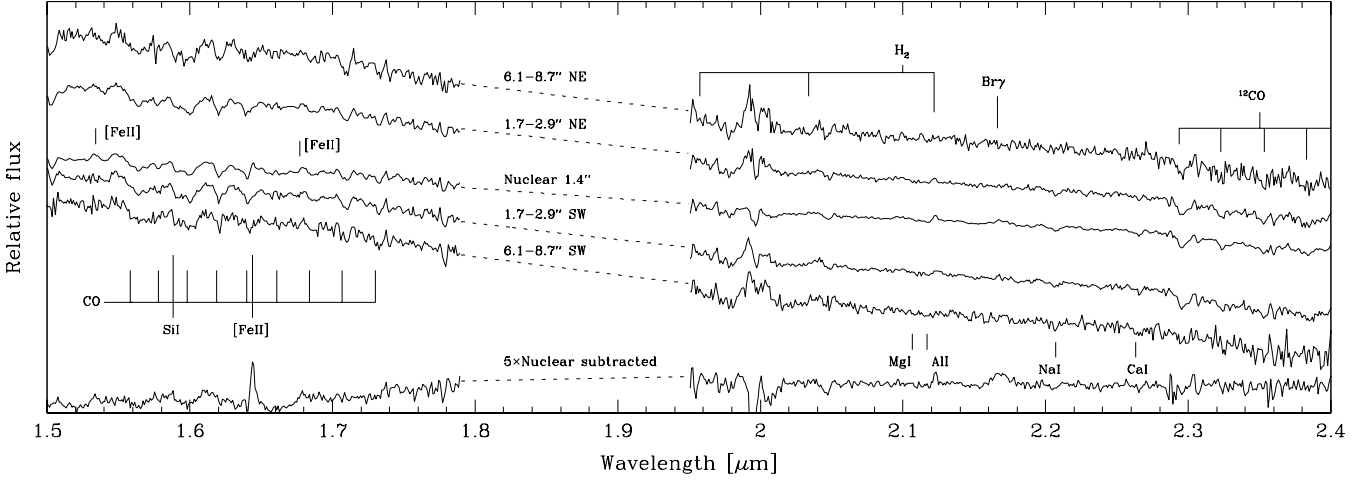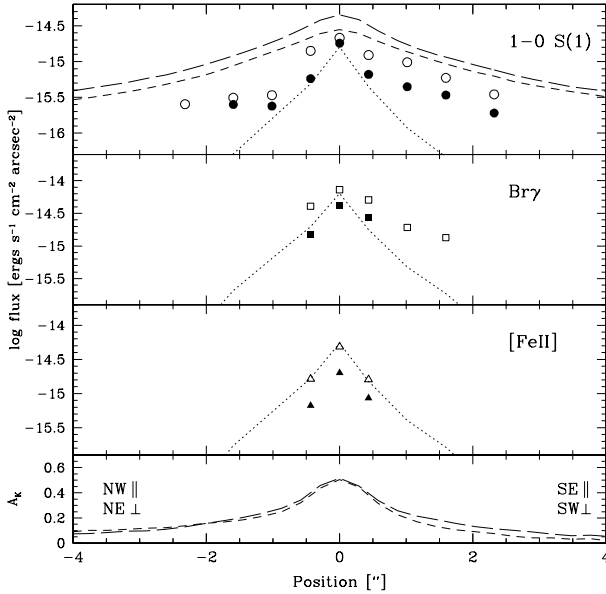
3.3 NGC 1566

NGC 1566 is a nearby (distance = 19 Mpc) barred (PA$\sim 0°$; Mulchaey, Regan, & Kundu 1997), ringed (diameter 1.7-kpc) SAB(s)bc galaxy in the Dorado group with a Sy1 nucleus. The nucleus in the high resolution [O III] map of Schmitt & Kinney (1996) is almost point-like, with maximum extent of $0''\!.7$ (59 pc). The [O III] map also shows conical extended emission in SE. To our knowledge, no NIR spectroscopy has previously been obtained for NGC 1566. The 1.5–2.5 μm spectrum is displayed in Fig. 10.

Both the line and the continuum emission appear much weaker parallel to the cone than perpendicular to it (Fig. 11). Of the lines detected in NGC 1566 neither [Fe II] nor Brγ are spatially resolved. The 1–0 S(1) emission is detected up to $\sim 2''$ ($\sim$200 pc in the plane of the galaxy) from the nucleus parallel to the cone and $\sim$ 280 pc perpendicular to it. The intrinsic spatial FWHM of the nuclear 1–0 S(1) emission is $\sim 1''\!.3$ perpendicular to the cone and $\sim 1''\!.2$ parallel to the cone. The 1–0 S(1) and [Fe II] lines are rather narrow, with intrinsic FWHMs 430 km s^{-1} and 600 km s^{-1} in the nuclear $1''\!.4$ aperture. The width of the 1-0 S(1) line is roughly constant along the slit, with no detectable difference between the two PAs.

The Brγ emission line is broad (Fig. 8), with FWHM = 2100 km s^{-1} in the combined nuclear $1''\!.4$ aperture after subtracting the neighbouring absorption lines. It is detected,

Table 4. Observed fluxes, reddening-corrected fluxes, gaussian FWHMs and equivalent widths for the various H_2 emission lines in the two extended regions in NGC 1386

Line	Region A observed 10^{-16} ergs s^{-1} cm^{-2}	corrected	FWHM Å	EW Å	Region B observed 10^{-16} ergs s^{-1} cm^{-2}	corrected	FWHM Å	EW Å
1-0 S(2)	7.0±01.0	7.3	25.6±3.2	3.0±0.5	14.6±1.0	16.1	23.8±1.2	2.8±0.2
1-0 S(1)	19.5±0.8	20.1	24.6±1.0	8.8±0.4	35.7±0.8	39.0	26.7±0.6	7.3±0.2
1-0 S(0)	4.2±0.7	4.3	20.4±3.9	2.2±0.4	6.8±0.7	7.4	21.3±2.3	1.5±0.2
2-1 S(1)	<2.3	<2.4	–	<1.2	<2.4	<2.7	–	<0.6
1-0 Q(1)	17±2	18	22.7±1.6	15±2	29±2	31	21.9±1.4	10.8±0.6
1-0 Q(3)	134±2	14	22.8±1.5	12±2	26±2	28	22.7±1.3	10.1±0.5

Figure 10. The 1.5–2.5 μm spectra of NGC 1566 perpendicular to the ionization cone.

Figure 11. The observed line emission in NGC 1566. The panels and symbols are as in Fig. 7, except the continuum emission is multiplied by a factor of 5.

however, only within the central $1''$, with no extended emission. The nuclear [Fe II] line is narrow (FWHM = 600 km s^{-1}), while there appears to be no narrow component to Brγ. Similarly, there is no broad component to the [Fe II] line, which can be explained if extinction $A_{2.2} > 3$ mag. However, the lack of the narrow Brγ component indicates a different excitation mechanism for iron, possibly X-ray excitation outside the BLR. The [Fe II] line is not spatially resolved, in agreement with the X-ray heating models by Krolik & Lepp (1989), which predict heating within the torus on scales of a few pc.

The H_2 2–1 S(1) line was not detected in the nucleus of NGC 1566, with 2–1 S(1)/1–0 S(1) $\leqslant 0.17$ (corresponding to $T_{vib} \leqslant 2700$ K), significantly less than predicted for UV fluorescence. The 1-0 S(1)/Brγ ratio is 0.27, suggesting thermal UV heating. The [Fe II]/Brγ ratio is 0.50, but since Brγ does not display a narrow component, a starburst contribution to the UV excitation cannot be larger than $\sim$10%. Therefore, it seems that the dominant mechanism for the excitation of the H_2 gas is collisional via shocks. The integrated mass the of excited molecular hydrogen along the direction of the ionization cone is $\sim$90 M$_\odot$ and perpendicular to it $\sim$110 M$_\odot$. The 1–0 S(1) velocity field (Fig. 9) appears relatively ordered, with increasing velocities with radius, thus suggesting that circular motions dominate the kinematics.
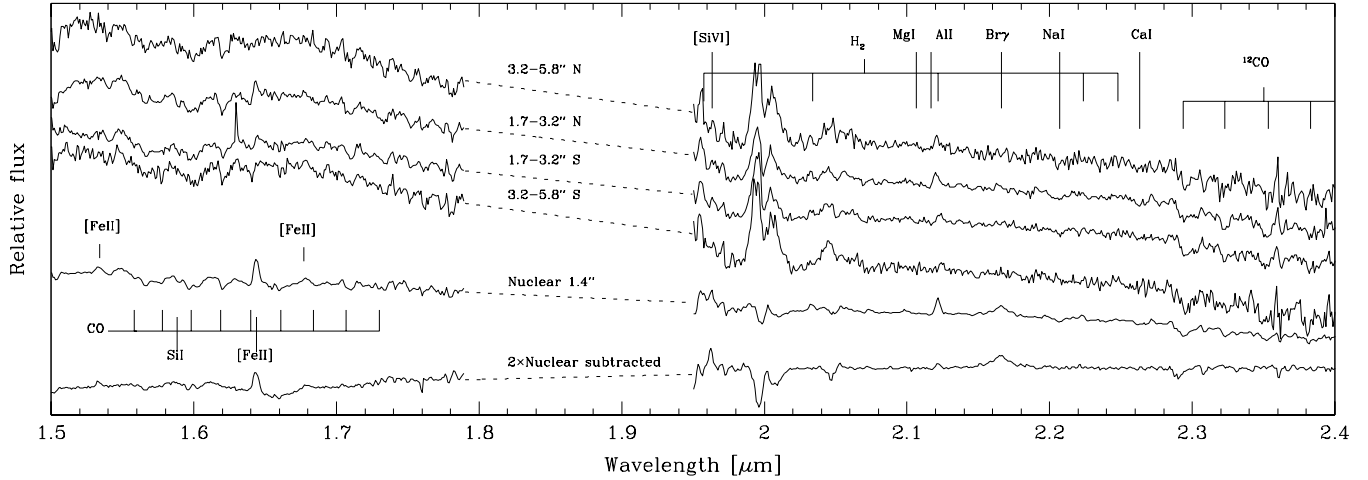
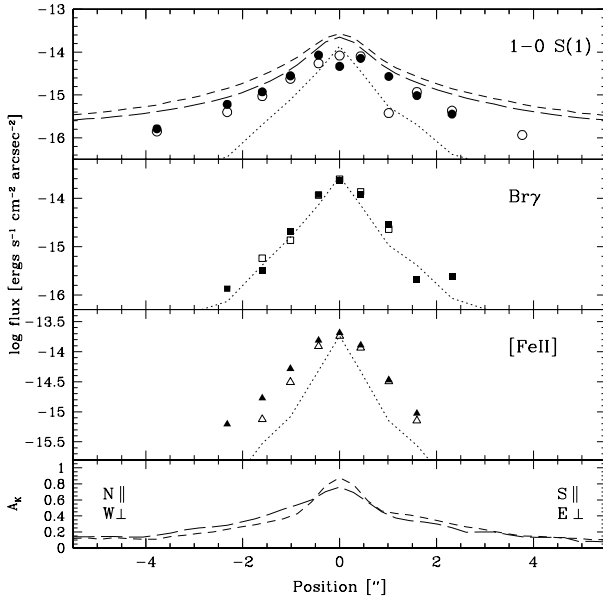**Figure 12.** The 1.5–2.5 μm spectra of NGC 3227 parallel to cone

Figure 13. The spatial extent of the three main emission lines in NGC 3227. For panels and symbols, see Fig. 7

Figure 14. The Brγ line profile of NGC 3227. Fit is obtained with a narrow component (FWHM = 650 km s^{-1}, flux 4.2×10^{-15}ergs cm^{-2} s^{-1}), and a broad component (FWHM = 2700 km s^{-1}, flux 23×10^{-15}ergs cm^{-2} s^{-1}).

3.4 NGC 3227

NGC 3227 is a nearby (distance = 15 Mpc) barred (Mulchaey et al. 1997; PA $\sim 150°$) SAB galaxy hosting a Sy1.5 nucleus with a one-sided cone to the N (Schmitt & Kinney 1996). It has been imaged with HST in the 1–0 S(1) and 1–0 S(3) lines by Quillen et al. (1999), although the very strong nuclear emission complicates subtracting the continuum in the centre. Recently, NIR spectroscopy of NGC 3227 has been obtained by Rhee & Larkin (2000; $R = 550$) and Schinnerer, Eckart & Tacconi (2001; $R = 700\text{-}1000$). In our new spectra the EW of [Fe II] and 1–0 S(1), and the integrated colours are in good agreement with those derived by Schinnerer et al. On the other hand, Brγ is much stronger and broader (EW = 8.3 Å; FWHM = 1800 km s^{-1}) in our
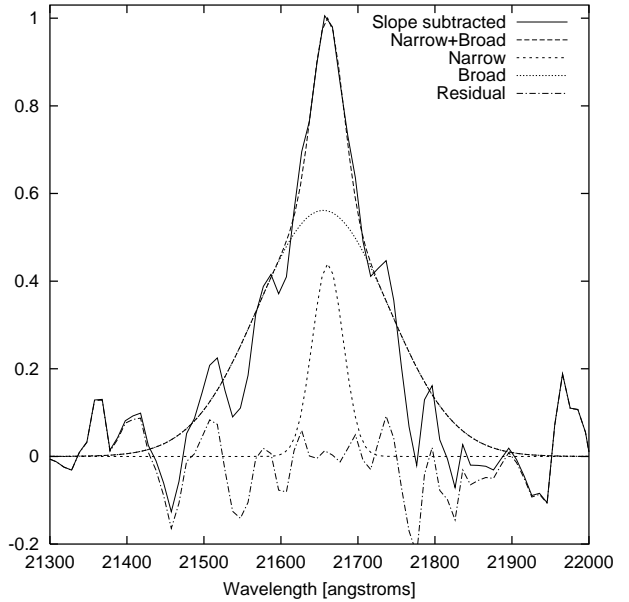
spectra than in those by Schinnerer et al. (EW = 3.7 Å; FWHM = 650 km s^{-1}).

Schinnerer et al. (2001) reported the detection of two coronal lines, [Si VI] and [Al IX] 2.043 μm. After subtracting the off-nuclear spectra to reduce the residual telluric lines, we found no evidence for the presence of [Al IX] (Fig. 12). The [Si VI] line is present, but at a much weaker level than reported by Schinnerer et al. However, this result is hardly conclusive because of the atmospheric signatures.

The Brγ line is broad in NGC 3227 (Fig. 8), with single component FWHM = $\sim$1800 km s^{-1}, in agreement with the results by Rhee & Larkin (2000). Unfortunately, outside the nucleus the S/N ratio in our spectra is not sufficiently high

to accurately subtract the continuum and determine the line profile, in the presence of neighbouring absorption lines (e.g. 2.1770 μm and 2.1460 μm). Fixing the narrow component at FWHM = 650 km s^{-1}, as derived by Schinnerer et al. (2001), the FWHM of the broad component is 2500 – 3000 km s^{-1} (Fig. 3.4), similar to that derived by Rhee & Larkin (2000).

The nuclear Brγ emission is spatially unresolved (Fig. 13), with no evidence for extended emission. Therefore, no recent star formation has been occurring in the disc of NGC 3227. However, Schinnerer et al. (2001) detected a young (25–50 Myr) star cluster close to the nucleus, which may already have passed the ionizing stage. Alternatively, it may be the origin of the narrow Brγ component. Neither 1–0 S(1) nor [Fe II] have broad profiles, indicating that Brγ originates much closer to the central engine than [Fe II]. The [Fe II] line is broader in the direction of the cone than perpendicular to it, and extends predominantly towards N. This effect may be due to line splitting, which is not directly detectable with our spectral resolution. The narrow [Fe II]/narrow Brγ ratio is $\sim$7.8, which suggests that the narrow nebular lines are excited by X-rays, as in the case of NGC 1386 or NGC 1566 (see above). Unlike in these galaxies, however, [Fe II] is spatially resolved in NGC 3227.

The nuclear 2–1 S(1)/1–0 S(1) ratio is 0.08, clearly ruling out UV fluorescence as the dominant excitation mechanism. Outside the nucleus, 1–0 S(1)/Brγ ratio $\gg$ 1, suggesting shocks to be responsible for the excitation of H$_2$. In the nuclear 1$''$.4 aperture, the gas density $N_{H_2} = 23.4\,10^{17}$ cm^{-2}, corresponding to gas mass of 280 M$_\odot$, in agreement with the mass 380 M$_\odot$ derived by Fernandez et al. (1999) from the peak H$_2$ surface brightness.

Both the 1–0 S(1) emission and, more marginally, the [Fe II] emission are spatially resolved, with no clear difference in the nuclear extent in the directions parallel and perpendicular to the cone. In the 1–0 S(1) image by Quillen et al. (1999) the emission is elongated along PA $\sim$ 100°. The 1–0 S(1) line is broader parallel to the ionization cone than perpendicular to it, similarly to [Fe II]. This suggests that both the excited H$_2$ and [Fe II] are emitted from the surface of the hollow ionization cone. In Schinnerer et al. (2001), the [Fe II] line was not spatially resolved, but this may be due to their poorer spatial resolution ($\sim$1$''$.6).

The velocity field is well-ordered and resembles solid rotation, especially parallel to cone, and [Fe II] appears to have the same dynamics as that of 1–0 S(1). Perpendicular to the cone the curve is noisier and flat.

3.5   NGC 4945

NGC 4945 is a nearby SB(s)cd galaxy in the Centaurus group of galaxies, with a dust lane SE of the nucleus. NGC 4945 has strong starburst activity, concentrated in a circumnuclear ring (Marconi et al. 2000) with a projected major axis diameter $\sim$ 11$''$ (210 pc). NGC 4945 also harbours a Sy2 nucleus, based on the detection of a heavily obscured, rapidly variable, strong hard X-ray source above 10 kev (Iwasawa et al. 1993), which is completely obscured below 10 kev. In the following we have adopted a distance of 3.9 Mpc for NGC 4945 (Harris, Poole & Harris 1998). The hollow cone, which may be produced by a superwind (e.g. Heckman, Armus & Miley 1990) from the powerful starburst and

not represent an outflow from the nucleus, is well visible in shorter wavelengths ($\lambda < 2\mu$m), especially NW of the nucleus (Moorwood et al. 1996).

Marconi et al. (2000) presented Paα, 1–0 S(1) and [Fe II] images of NGC 4945. Our new data (Figs. 15, 16) are in good agreement with their results. The Paα image of Marconi et al. shows no central peak but is dominated by a star forming ring. In the superwind direction, the two Brγ maxima separated by $\sim$2$''$ (180 pc in the plane of the galaxy) correspond to the SE and NW parts of the ring. The [Fe II] emission in our spectra is also in good agreement with that in Marconi et al. The NW peak at $\sim$5$''$ (440 pc) from the nucleus appears as an elongation in their image. The [Fe II] emission can be traced further out toward NW than SE. Another tracer of young stars, He I can be traced $\sim$6–8$''$ ($\sim$230 pc) from the nucleus perpendicular and $\sim$3$''$ (260 pc) parallel to the superwind. The 1–0 S(1) map in Marconi et al. shows an elongated (PA$\sim$ 33°) nuclear emission and extended emission to SW and NW of the nucleus, in agreement with our spectra. Toward SW, the emission rapidly decreases with local peaks at 4$''$ (130 pc) and 7$''$ (230 pc) distance, while toward NE the decline is slower.

There are quite large radial changes in the line ratios of the main emission lines relative to 1–0 S(1) (Fig. 17). Notably, the star forming region SW of the nucleus perpendicular to the superwind is clearly visible. There is a reasonable correlation between Brγ and He I, while the behaviour of [Fe II] emission is different from them. The Brγ/1–0 S(1) ratio is 0.1–0.5 toward NE and NW of the nucleus, suggesting that UV heating is not important. However, toward SE this ratio is $\sim$1.0 at 2$''$ (180 pc) distance from the nucleus and toward SW it is $\sim$1.4 at 5$''$ (160 pc) distance from the nucleus. These ratios indicate, together with the enhanced He I and [Fe II] emission, that UV emission from young, hot stars is important.

The 2–1 S(1)/1–0 S(1) ratio of $\sim$0.1–0.2 (Fig. 17) is in good agreement with collisional excitation at $T_{vib} = 2000 - 2500$ K. The 1–0 Q(1)/1–0 Q(3) ratio in the nucleus is $\sim$1, and the associated rotational temperature $T_{rot} \simeq 2000$ K. Adopting $T = 2000$ K, the density of excited H$_2$ in the nucleus $N_{H_2} \simeq 100 \times 10^{17}$ cm^{-2} (corresponding to $m \simeq 70$ M$_\odot$), much lower than the available mass of warm ($T = 160$ K) H$_2$ (2.4$\times$10^7 M$_\odot$; Spoon et al. 2000).

The [Fe II]/Brγ ratio of $\sim$ 4.5 at the nucleus (Fig. 17) is lower than expected for X-ray excitation and can better be explained by shocks and star formation. Perpendicular to the superwind, the He I/Brγ ratio is roughly constant, with slightly larger ratios ($\sim$0.4) toward NE than SW. However, $\sim$1–3$''$ SW there is a region with significantly lower ratios ($\sim$0.1–0.2). This may be due to a lower number of high mass stars as a result of a decaying starburst or a truncated IMF in this region. Parallel to the superwind, this ratio is higher, $\sim$ 0.8, both 1$''$ NW and 0$''$.5 SE of the nucleus.

Both the 1–0 S(1) and especially the [Fe II] are significantly broader in the direction of the superwind (up to 550 km s^{-1} and 700–800 km s^{-1}, respectively) than perpendicular to it ($\sim$ 400 km s^{-1}) at $\sim$5$''$ (440 pc) distance from the nucleus. This is in agreement with that observed in Hα (Heckman et al. 1990). However, [Fe II] and 1–0 S(1) are also broader SE of the nucleus unlike Hα, probably due to lower extinction which in NIR makes it possible to observe the cone surface furthest from us.
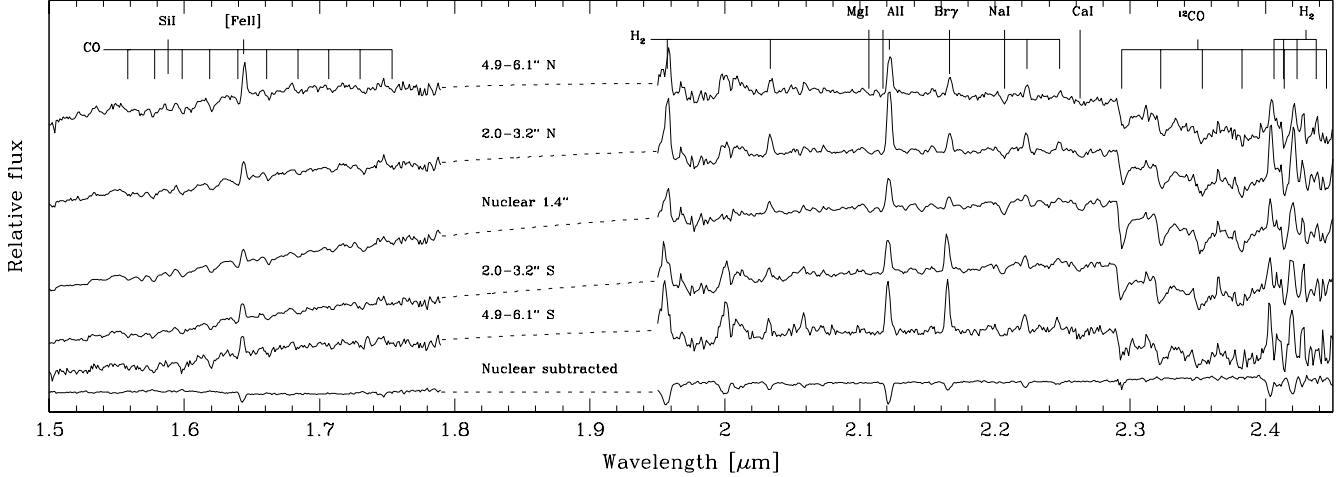
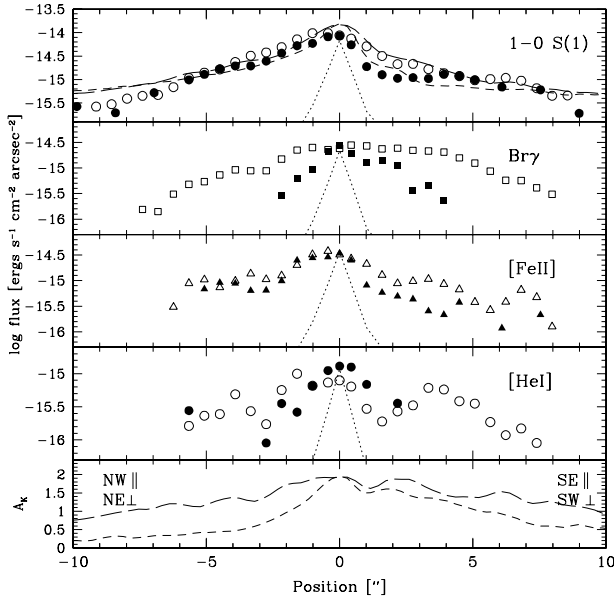**Figure 15.** The $1.5 - 2.5$ μm spectra of NGC 4945 perpendicular to the superwind.

Figure 16. The observed line emission in NGC 4945. The panels and symbols are as in Fig. 7.

Figure 17. The line ratios of the main emission lines with respect to 1–0 S(1) in NGC 4945.

The 1–0 S(1) emission has a red wing within a few central arcsec, but it is symmetric further out. On the other hand, SW of the nucleus, the red wing in both Brγ and [Fe II] is much stronger than the blue wing, while NE of the nucleus the blue wing is stronger. A likely explanation for this behaviour is that the line-of-sight rotational velocity in the nuclear ring is higher than in the underlying galaxy, either intrinsically or as a result of the ring inclination with respect to the galaxy.

Both perpendicular and parallel to the superwind, the velocity field (Fig. 18) of 1–0 S(1) is clearly different from that of [Fe II] and Brγ, suggesting differences in the dynamics and/or excitation mechanism. The kinematics of Brγ and [Fe II] are better correlated, except toward NE of the nucleus.
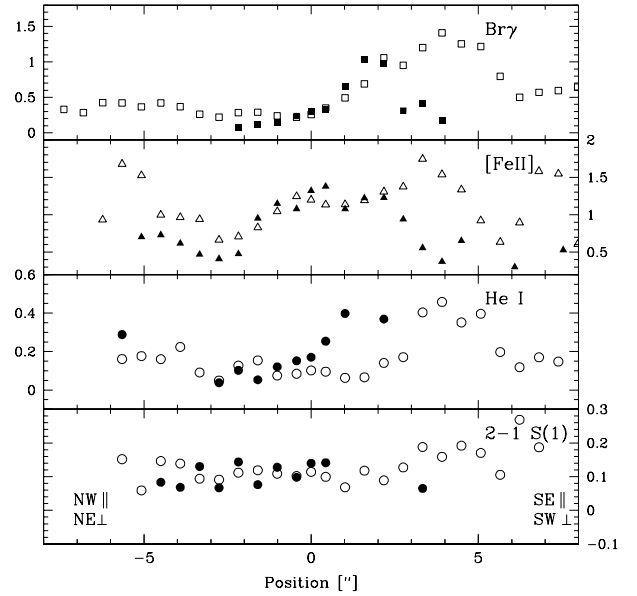
1–0 S(1) follows better the stellar rotation as derived from absorption lines than from either Brγ or [Fe II], but correlation is not perfect. The most intriguing feature is the roughly sinusoidal form of the rotation curve in the direction of the superwind. It is most clearly seen in the various H$_2$ lines, but is also present in Brγ and He I. Based on the velocity field of [Fe II] and assuming $i = 78° \pm 2°$ and position angle for the line of nodes $PA = 43° \pm 1°$ (Ables et al. 1987), we derive a dynamical mass $M_{\rm dyn} = 3.2 \times 10^8 M_\odot$. This value is slightly less than that derived in the inner $R \leqslant 100$pc from millimeter CO observations ($M_{\rm dyn} \sim 8 \times 10^8 M_\odot$; Mauersberger et al. 1996).
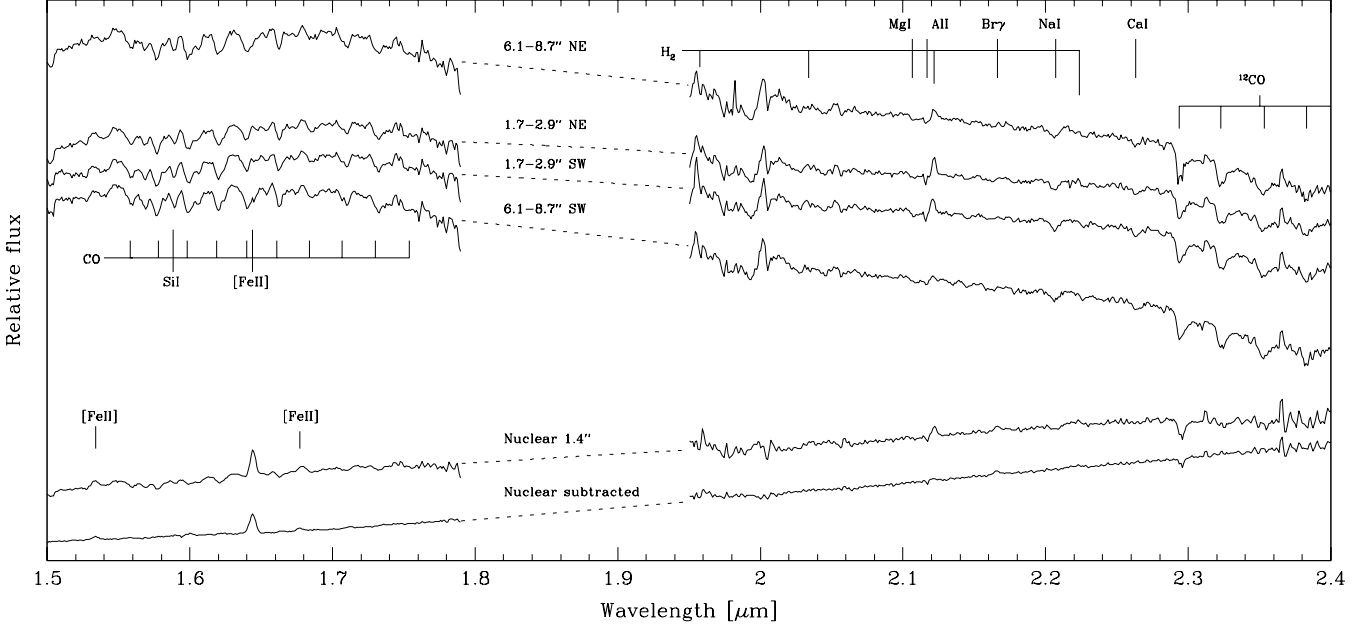
Figure 19. The 1.5–2.5 μm spectra of NGC 5128 perpendicular to the jet.
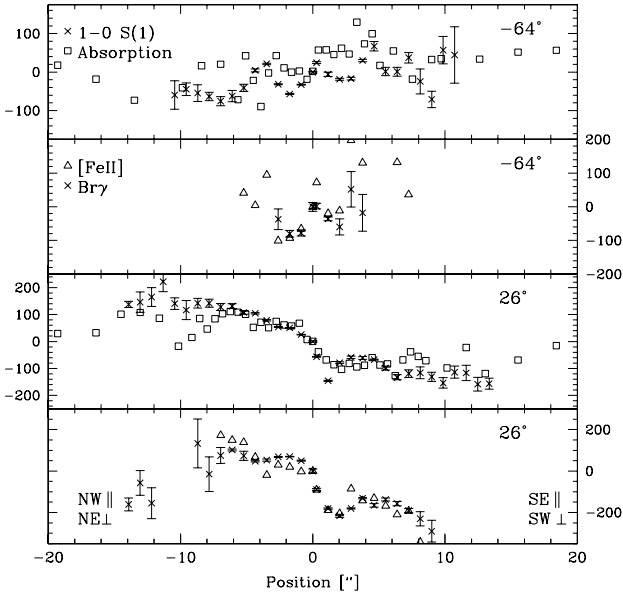

Figure 18. The velocity field of the main emission lines and the K-band CO-absorption lines in NGC 4945 parallel to the superwind (-64°) and perpendicular to it (26°) in the units of km s^{-1}.

3.6 NGC 5128

NGC 5128 (Centaurus A) is a well-studied galaxy with prominent dust lanes (e.g. Schreier et al. 1996) and Sy2 nucleus. It has very prominent radio jets which after 5-kpc expand into plumes. The distance of NGC 5128 has been controversial, with estimates ranging from 2.1 Mpc to 8.5 Mpc; in the following, we have adopted the distance of 3.9

Mpc (Harris et al. 1998). Previous NIR spectroscopic studies of NGC 5128 include e.g. Marconi et al. (2001) and Bryant & Hunstead (1999). In addition, it has been the target of NIR Paα (Schreier et al. 1998) and [Fe II] (Marconi et al. 2001) imaging. For a comprehensive review of NGC 5128, see Israel (1998).

The spectra of NGC 5128 at different distances from the nucleus perpendicular to the jet are displayed in Fig. 19. The subtracted nuclear spectrum is almost featureless. There are some notable differences between our spectra and those from the literature. Especially, while the nuclear $1''.4 \times 1''.6$ [Fe II]/Brγ ratio observed by Simpson & Meadows (1998) = 1.47, we find this ratio to be 5.1, and after correction for extinction even $\sim$15, one of the largest ratios ever found.

The most striking feature in the spectra of NGC 5128 is the weakness of the line emission compared to that in NGC 4945 at similar distance. This is partly due to dilution by the bright, red, featureless nuclear continuum. [Fe II] is the strongest line in the nuclear region. However, the only emission line that can be traced out into the galaxy is 1–0 S(1) (Fig. 20), which extends parallel to the jet up to $13''.4$ (320 pc in the plane of the galaxy) in NE and $7''.4$ (180 pc) in SW, and perpendicular to the jet up to $16''$ (690 pc) in NW and $22''$ (950 pc) in SE. The nuclear Brγ emission is not spatially resolved. In the deeper K-band spectra of Marconi et al. (2001) the nucleus is resolved and detected up to $1''$ from the nucleus. Marconi et al. interpreted this as an inclined, $\sim$40 pc diameter, thin disc of ionized gas. In addition to central component, there are a few star forming regions parallel to the jet visible in our spectra, e.g. at $\sim$17$''$ (400 pc) with detected Brγ and [Fe II] emission. This is in agreement with the Paα and [Fe II] images of Schreier et al (1998) and Marconi et al. (2001), respectively, which display two extended regions straddling the nucleus at PA $\sim$33°.
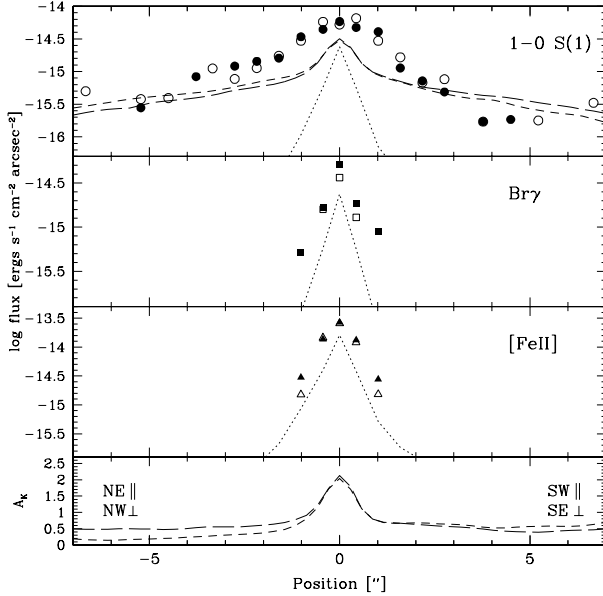
Figure 20. The observed line emission in NGC 5128. Symbols are as in Fig. 7

The [Fe II]-emission of Marconi et al. is mostly unresolved with faint extended emission NW of the nucleus.

No 2–1 S(1) emission was detected in the nucleus, with an upper limit of 2–1 S(1)/1–0 S(1) $\leqslant 0.08$ ($T_{\rm vib} < 1900$ K). Since the 1–0 S(1)/Brγ ratio is 2.04, the H_2 gas is probably excited by shocks. Assuming $T_{\rm vib} = 2000K$, the density of H_2 is 45.6×10^{17} cm^{-2}, corresponding to a gas mass of 33.8 $M_\odot$.

Our velocity field for NGC 5128 is displayed in Fig. 9. It is in agreement with Marconi et al. (2001), but unfortunately we lack the necessary resolution or depth to supplement their results.

4 CONCLUSIONS

We have presented NIR 1.5–2.5 μm long-slit spectra of six Seyfert galaxies with an ionization cone or jets. While statistical analysis will be presented in forthcoming papers using the full sample of 14 Seyferts, some general trends can already be noted. [Fe II] is the strongest and Brγ the weakest main emission line in the Sy2s NGC 1386, NGC 4945 and NGC 5128. On the other hand, in the Sy1 NGC 1097 1–0 S(1), and in the Sy1 NGC 1566 and the Sy1.5 NGC 3227 Brγ is the strongest emission line. Brγ was not detected in the nucleus of NGC 1097. Notably, in NGC 1386 the coronal [Si VII] line is even stronger than [Fe II], [Si VI] is comparable to [Fe II] and [Ca VIII] is stronger than Brγ. In addition, [Si VI] and [Si VII] were also detected in NGC 3227.

Broad nuclear Brγ line emission was detected in NGC 1386, NGC 1566 and NGC 3227, in which narrow Brγ component is only visible in NGC 3227. Based on the high [Fe II]/Brγ-ratios it seems probable that [Fe II] is X-ray excited. The [Fe II] emission is spatially resolved only in NGC 3227 and NGC 4945, which also agrees with the theory of

X-ray excitation in NLR as the origin for the [Fe II] emission (e.g. Mouri, Kawara & Taniguchi 2000).

The 1–0 S(1) emission is extended in all galaxies, except parallel to the cone in NGC 1386. The extended 1–0 S(1) emission can be detected up to a range of physical scales, from ~ 200 pc in the plane of the galaxy in NGC 1097 to $\sim$1.4-kpc in NGC 4945. In NGC 1097, NGC 1386 and NGC 4945 separate off-nuclear 1–0 S(1) emission regions are detected. In NGC 1097 and NGC 4945 these regions are associated with the starburst rings, while in NGC 1386 the origin of these regions remains unknown, but are likely to be connected with a nuclear outflow. Since the extended emission declines smoothly with increasing radius, it seems probable that the molecular gas forms a disc surrounding the nucleus. This is further supported by 1–0 S(1) velocity curves, which are generally well-ordered except parallel to the superwind in NGC 4945. A starburst origin seems excluded as extended Brγ or [Fe II] is only detected in NGC 1097 and NGC 4945. In these galaxies, the extended emission is associated with off-nuclear star forming regions

The overall 1–0 S(1) emission is more extended parallel to the cone/jet than perpendicular to it in NGC 1097, NGC 1386 and NGC 4945, while the opposite is true in NGC 3227, NGC 1566 and NGC 5128, so the total extent of the emission does not depend on the type of the nucleus. The extent of the nuclear core H_2 emission is larger perpendicular to the ionization cone/jet than parallel to it in NGC 1097, NGC 1386, NGC 1566, NGC 3227 and NGC 4945, in good agreement with the current unified models and the existence of a molecular torus. In NGC 5128, on the other hand, the extent is larger parallel to the jet than perpendicular to it.

There does not appear to be a clear difference between the gas mass M_{H_2} parallel and perpendicular to the ionization cone. In NGC 1566, NGC 3227, and especially in NGC 4945, M_{H_2} parallel to the cone is smaller than perpendicular to it. On the other hand, in NGC 5128 the two masses are similar, while in NGC 1097 and NGC 1386 M_{H_2} parallel to the cone/jet is larger than perpendicular to it. The highest nuclear gas densities N_{H_2} are found in the Sy2s NGC 4945 and NGC 5128, and the lowest in the Sy1s NGC 1097 and NGC 1566. In the Sy1.5 NGC 3227 the density is intermediate, while in the Sy2 NGC 1386 the density is comparable to that in the Sy1s.

In all galaxies, the dominant excitation mechanism of the nuclear H_2 emission appears to be due to shocks. No evidence for significant UV fluorescence was found. The extended H_2 emission in NGC 1097, NGC 1386 and NGC 4945 is also best explained by thermal excitation.

5 ACKNOWLEDGEMENTS

References:

Ables J.G., Forster J.R., Manchester R.N. et al., 1987, MNRAS, 226, 157

Alonso-Herrero A., Rieke M.J., Rieke G.H., Ruiz M., 1997, ApJ, 482, 747

Antonucci R., 1993, ARA&A, 31, 473

Bryant J.J., Hunstead R.W., 1999, MNRAS, 308, 431

Contini M., Viegas S.M., 2001, ApJS, 132, 211

Fernandez B.R., Holloway A.J., Meaburn J., Pedlar A., Mundell C.G., 1999, MNRAS, 305, 319

Fioc M., Rocca-Volmerange B., 1999, A&A, 351, 869

Gredel R., Dalgarno A., 1995, ApJ, 446, 852

Harris G.L.H., Poole G.R., Harris W.E., 1998, AJ, 116, 2866

Heckman T.M., Armus L., Miley G.K., 1990, ApJS, 74, 833

Hollenbach D., McKee C.F., 1989, ApJ, 342, 306

Hunt L., Malkan M.A., Salvati M., et al., 1997, ApJS, 108, 229

Israel F.P., 1998, A&AR, 8, 237

Iwasawa K., Koyama K., Awaki H., et al., 1993, ApJ, 409, 155

Kotilainen J.K., Reunanen J., Laine S., Ryder S., 2000, A&A, 353, 834

Krolik J.H., Lepp S., 1989, ApJ, 347, 179

Landini M., Natta A., Salinari P., Oliva E., Moorwood A.F.M., 1984, A&A, 134, 284

Lidman C., Cuby J.-G., Vanzi L., 2000 SOFI User's manual, LSO-MAN-ESO-40100-0003

Maiolino R., Ruiz M., Rieke G.H., Papadopoulos P., 1997, ApJ 485, 552

Malkan M.A., Gorjian V., Tam R., 1998, ApJS, 117, 25

Maloney P.R., Hollenbach D.J., Tielens G.G.M., 1996, ApJ, 466, 561

Marconi A., van der Werf P.P., Moorwood A.F.M., Oliva E., 1996, A&A, 315, 335

Marconi A., Schreier E.J., Koekemoer A., et al., 2000, ApJ, 528, 276

Marconi A., Capetti A., Axon D., et al., 2001, ApJ, 549, 915

Mauersberger R., Henkel C., Whiteoak J.B., Chin Y.-N., Tieftrunk A.R., 1996, A&A, 309, 705

Moorwood A.F.M., Oliva E. 1988, A&A, 103, 278

Moorwood A.F.M., van der Werf P.P, Kotilainen J.K., Marconi A., Oliva E. 1996, A&A, 308, 1L

Moran E.C., Barth A.J., Kay L.E., Filippenko A.V., 2000, ApJ, 540, L73

Mouri H., Kawara K., Taniguchi Y., 2000, ApJ, 528, 186

Mulchaey J.S., Wilson A.S., Tsvetanov Z., 1996, ApJ, 467, 197

Mulchaey J.S., Regan M.W., Kundu A., 1997, ApJS, 110, 299

Nagar N.M., Wilson A.S., Mulchaey J.S., Gallimore J.F., 1999, ApJS, 120, 209

Oliva E., Salvati M., Moorwood A.F.M., Marconi A., 1994, A&A, 288, 457

Phillips M.M. Pagel B.E., Edmunds M.G., Diaz A., 1984, MNRAS, 210, 701

Quillen A.C., Alonso-Herrero A., Rieke M.J., et al., 1999, ApJ, 527, 696

Rhee J.H., Larkin J.E., 2000, ApJ, 538, 98

Rossa J., Dietrich M., Wagner S.J., 2000, A&A, 362, 501

Schinnerer E., Eckart A. Tacconi L.J., 2001, ApJ, 549, 254

Schmitt H.R., Kinney A.I., 1996, ApJ, 463, 498

Schreier E.J., Capetti A., Macchetto F., Sparks W.B., Ford H.J., 1996, ApJ, 459, 535

Schreier E.J., Marconi A., Axon D., et al. 1998, ApJ, 499, L143

Scoville N.Z., Hall D.N.B., Kleinmann S.G., Ridgway S.T., 1982, ApJ, 253, 136

Simpson C., Meadows V., 1998, ApJ, 505, L99

Spoon H.W.W., Koornneef J., Moorwood A.F.M., Lutz D., Tielens A.G.G.M., 2000, A&A, 357, 898

Sternberg A., Dalgarno A., 1989, ApJ, 338, 197

Storchi-Bergmann T., Baldwin J.A., Wilson A.S., 1993, ApJ, 410, 11

Storchi-Bergmann T., Wilson A.S., Baldwin J.A., 1996a, ApJ, 460, 252

Storchi-Bergmann T., Rodríguez-Ardila A, Schmitt H.R., Wilson A.S., Baldwin J.A., 1996b, ApJ, 472, 83

Storchi-Bergmann T., Winge C., Ward M.J., Wilson A.S., 1999, MNRAS, 304, 35

Turner J., Kirby-Docken K., Dalgarno A., 1977, ApJS, 35, 281

Veilleux S., Goodrich R.W., Hill G.J., 1997, ApJ, 477, 631

Weaver K.A., Wilson A.S., Baldwin J.A., 1991, ApJ, 366, 50

Wehrle A.E., Keel W.C., Jones D.L., 1997, AJ, 114, 115

Winge C., Storchi-Bergmann T., Ward M.J., Wilson A.S., 2000, MNRAS, 316, 1

Wolstencroft R.D., Tully R.B., Perley R.A., 1984, MNRAS, 207, 889